Thermal–Mechanical Coupled Analysis of a Brake Disk Rotor

Article *in* Heat and Mass Transfer · April 2013

DOI: 10.1007/s00231-013-1161-8

2 authors:

Ali Belhocine
Université des Sciences et de la Technologie d'Oran Mohamed Boudiaf
225 PUBLICATIONS **805** CITATIONS
SEE PROFILE

Mostefa Bouchetara
Université des Sciences et de la Technologie d'Oran Mohamed Boudiaf
63 PUBLICATIONS **439** CITATIONS
SEE PROFILE

Thermal–mechanical coupled analysis of a brake disk rotor

Ali Belhocine & Mostefa Bouchetara

Heat and Mass Transfer
Wärme- und Stoffübertragung

ISSN 0947-7411
Volume 49
Number 8

Heat Mass Transfer (2013) 49:1167-1179
DOI 10.1007/s00231-013-1161-8

Springer

Heat Mass Transfer (2013) 49:1167–1179
DOI 10.1007/s00231-013-1161-8

ORIGINAL

Thermal–mechanical coupled analysis of a brake disk rotor

Ali Belhocine · Mostefa Bouchetara

Received: 15 August 2012 / Accepted: 22 April 2013 / Published online: 4 May 2013

Abstract The main purpose of this study is to analyze the thermomechanical behavior of the dry contact between the brake disk and pads during the braking phase. The simulation strategy is based on computer code ANSYS11. The modeling of transient temperature in the disk is actually used to identify the factor of geometric design of the disk to install the ventilation system in vehicles The thermal–structural analysis is then used with coupling to determine the deformation and the Von Mises stress established in the disk, the contact pressure distribution in pads. The results are satisfactory when compared to those of the specialized literature.

List of symbols

a	Deceleration of the vehicle (m/s^2)
A_d	Disk surface swept by a brake pad (m^2)
C_p	Specific heat (J/kg °C)
E	Young modulus (MPa)
g	Gravitational acceleration (m/s^2)
h	Heat transfer coefficient (W/m^2 °C)
k	Thermal conductivity (W/m °C)
k_d	Thermal conductivity of the disk (W/m °C)
k_g	Thermal conductivity of the pad (W/m °C)
m	Mass of the vehicle (kg)
q_0	Heat flux entering the disk (W)
q_x	Conduction heat flux in x direction (W/m^2)
q_y	Conduction heat flux in y direction (W/m^2)
q_z	Conduction heat flux in z direction (W/m^2)
Q	Internal heat generation rate per unit volume (W/m^3)
S_d	Disk surface (m^2)
S_g	Pad surface (m^2)
t	Time (s)
T	Temperature (°C)
T_1	Specified surface temperature (°C)
T_s	Unknown surface temperature (°C)
T_∞	Convective exchange temperature (°C)
v_0	Initial speed of the vehicle (m/s)
x	Space variable in x direction (m)
y	Space variable in x direction (m)
z	Space variable in x direction (m)
z	Braking effectiveness

Greek symbols

α	Thermal expansion coefficient (1/°C)
ε_p	Factor load distribution on the disk surface
υ	Poisson coefficient, dimensionless
ρ	Mass density (kg/m^3)
ρ_d	Density of the brake disk (kg/m^3)
ρ_g	Density of the pad (kg/m^3)
μ	Coefficient of friction, dimensionless
ϕ	Rate distribution of the braking forces between the front and rear axle
φ_c	Heat partition coefficient, dimensionless
ω	Angular velocity (rd/s)

Index

FG	Gray cast iron
CFD	Computational fluid dynamic

1 Introduction

The braking process is in fact the matter of energy balance. The aim of braking system is to transform mechanical

A. Belhocine · M. Bouchetara
Faculty of Mechanical Engineering, University of Sciences and the Technology of Oran (USTO), L.P 1505 El-Mnaouer, 31000 Oran, Algeria

A. Belhocine (✉)
29, Street Larbi Tebessi, Ain Fares, 29140 Oran, Algeria
e-mail: al.belhocine@yahoo.fr

energy of moving vehicle into some other form, which results in decreasing the speed of the vehicle. The kinetic energy is transformed into the thermal energy, by means of dry friction effects, which then is, dissipated into the surroundings [1].

The friction heat generated between two sliding bodies causes thermoelastic deformation which alters the contact pressure distribution. This coupled thermo-mechanical process is referred to as frictionally-excited thermoelastic instability or TEI [2]. If the sliding speed is above one called critical speed, the resulting thermo-mechanical feedback is unstable, leading to the development of non-uniform contact pressure and local high temperature with important gradients called 'hot spots' [3]. The formation of such localized hot spots is accompanied by high local stresses that can lead to material degradation and eventual failure [4]. Also, the hot spots can be a source of undesirable frictional vibrations, known in the automotive disk brake community as 'hot roughness' or 'hot judder' [5].

In 2002, Nakatsuji et al. [6] conducted a study on the initiation of hair-like cracks which are formed around small holes in the flanges of one-piece disks during overloading conditions. The study showed that thermally induced cyclic stress strongly affects the crack initiation in the brake disks. In order to show the crack initiation mechanism, the temperature distribution at the flange was firstly measured. The temperature distribution under overloading was analyzed by using the finite element method. Based on the experimental and calculated results, the crack initiation mechanism for one-piece brake disks at the very severe braking condition was explained. In addition, the effective methods are suggested for reducing the initiation of tiny cracks around the holes.

In 2000, Valvano and Lee [7] conducted a study of the technique to determine the thermal distortion of a brake rotor. The severe thermal distortion of a brake rotor can affect important brake system characteristics such as the system response and brake judder propensity. As such, the accurate prediction of thermal distortions can help in the designing of a brake disk.

In 1997, Hudson and Ruhl [8] conducted a study of the air flow through the passage of a Chrysler LH platform-ventilated brake rotor. Modifications to the production rotor's vent inlet geometry were prototyped and measured, in addition to the production rotor. Vent passage air flow was compared with the existing correlations. With the aid of Chrysler Corporation, investigation of ventilated brake rotor vane air flow was undertaken. The goal was to measure current vane air flow and to improve this vane flow to increase brake disk cooling. Temperature increases can strongly influence the properties of the surface of materials in slip, support physicochemical and microstructural transformations, and modify the rheology of interfacial elements trapped in the contact zone [9]. Recent numerical models, presented to deal with rolling processes [10, 11] have shown that the thermal gradients can attain important levels which depend on the heat dissipated by friction, the rolling speed, and the heat transfer coefficient. Many other studies [12, 13] dealt with the evaluation of temperature in solids subjected to frictional heating. The temperature distribution due to friction process necessitates a good knowledge of the contact parameters. In fact, the interface is always imperfect—due to the roughness—from mechanical and thermal points of view. Recently, theoretical and experimental studies [14, 15] have been developed to characterize the thermal parameters which govern the heat transfer at the vicinity of a sliding interface. In certain industrial applications, the solids are provided with a surface coating. A recent study has been carried out to analyze the effect of surface coating on the thermal behavior of a solid subjected to the friction process [16]. Increased thermal efficiency and the integrity of materials in high-temperature environments is an essential requirement in modem engineering structures in automotive, aerospace, nuclear, offshore, environmental, and other industries. Nowadays, the FE method is used regularly to obtain numerical solutions for heat transfer problems. The most common choice when using finite elements is the standard Galerkin formulation [17].

Gao and Lin [18] have presented an analytical model for the determination of the contact temperature distribution on the working surface of a brake. To consider the effects of the moving heat source (the pad) with relative sliding speed variation, a transient finite element technique is used to characterize the temperature fields of the solid rotor with appropriate thermal boundary conditions. Numerical results shows that the operating characteristics of the brake exert an essentially influence on the surface temperature distribution and the maximal contact temperature.

Talati and Jalalifar [19] presented a paper on Analysis of heat conduction in a disk brake system. In this paper, the governing heat equations for the disk and the pad are extracted in the form of transient heat equations with heat generation that is dependant to time and space. In the derivation of the heat equations, parameters such as the duration of braking, vehicle velocity, geometries and the dimensions of the brake components, materials of the disk brake rotor and the pad and contact pressure distribution have been taken into account. The problem is solved analytically using Green's function approach. It is concluded that the heat generated due to friction between the disk and the pad should be ideally dissipated to the environment to avoid decreasing the friction coefficient between the disk and the pad and to avoid the temperature rise of various brake components and break fluid vaporization due to excessive heating.

Naji et al. [20] presented a mathematical model to describe the thermal behavior of a brake system which consists of the shoe and the drum. The model is solved analytically using Green's function method for any type of the stopping braking action. The thermal behavior is investigated for three specified braking actions which were the impulse, the unit step and trigonometric stopping actions.

Thermal response of disk brake systems to different materials used for the disk–pad couple has been studied in many researches [21–28]. Aerodynamic cooling of high performance disk brake systems is investigated by many researchers [29–31].

Kang and Cho [32] was conducted to analyze the geometry of vents in motorcycle disk brakes which affects the surface of the disk. To analyze the thermal characteristics of disk brakes, thermal deformation analysis and thermal stress analysis due to heat transfer was carried out through the finite element analysis for ventilated disk and solid disk. For 3-dimensional modeling and finite element analysis of the disks, the commercial code ANSYS Workbench was used.

Thilak and Krishnaraj [33] conducted a transient thermal and structural analysis of a brake disk to evaluate its performance under severe braking conditions and there by assist in disk rotor design and analysis. The usage of new materials was investigated which aims at improving the braking efficiency and providing greater stability to the vehicle. This study was done using ANSYS 11 software to analyze the temperature distribution, variation of the stresses and deformation across the disk brake profile. The new materials under study were Aluminum base metal matrix composite and High Strength Glass Fiber composites. These materials have a promising friction and wear behavior as a brake disk. The transient thermo elastic analysis of disks in repeated brake applications was performed and the results were compared to that of cast iron disk.

In this study, we will make a modeling of the thermo-mechanical behavior of the dry contact between the disks of brake pads at the time of braking phase; the strategy of calculation is based on the software ANSYS 11 [34]. This last is comprehensive mainly for the resolution of the complex physical problems. The numerical simulation of the coupled transient thermal field and stress field is carried out by sequentially thermal-structurally coupled method based on ANSYS.

2 Heat flux entering the disk

In the case of disk brake, the effective friction processes between the pads and the disk are extremely complex because the present time brake pads, due to their composite structure [35], do not have constant chemical-physical properties, with the organic containing elements being subjected to a series of transformations under the influence of temperature increase. The heat distribution between the brake disk and the friction pads is mostly dependent on material characteristics, a major influence among which arises from the densities $\rho_{d,g}$ (kg/m^3), the thermal conductivities $k_{d,g}$ (W/m °C) and the specific heats $C_{d,g}$ (J/kg °C) of the disk's (subscript d), and the braking pad's materials, respectively (subscript g). Denoting Q_d and Q_g [J], as the heat quantities assumed by the disk and the braking pads, respectively, one can express in the following manner [36]:

$$\frac{Q_d}{Q_g} = \frac{\sqrt{\rho_d.k_d.C_d}}{\sqrt{\rho_g.k_g.C_g}} \tag{1}$$

Because the braking disk is not entirely covered by the friction pads, while computing, we have to consider the ratio between the disk surface S_d and the pad surface S_g. Denoting the ratio of heat's division between the disk and pads as:

$$\varphi_c = \frac{Q_d}{Q_g}.\frac{S_d}{S_g} = \frac{\sqrt{\rho_d.k_d.C_d}}{\sqrt{\rho_g.k_g.C_g}}.\frac{S_d}{S_g} \tag{2}$$

and considering Q [J] the heat quantity generated during the friction process, the heat quantities assumed by the pads and the disk are, respectively,

$$Q_g = Q.\frac{1}{1+\varphi_c} \tag{3}$$

$$Q_d = Q.\frac{\varphi_c}{1+\varphi_c} \tag{4}$$

Figure 1 shows the ventilated disk—pads and the applied forces. The geometrical characteristics of the ventilated disk are illustrated in Fig. 2.

The brake disk consumes the major part of the heat, usually grater than 90 % [37], by means of the effective contact surface of the friction coupling. Considering the complexity of the problem and the limitation in the average data processing, one identifies the pads by their effect, represented by an entering heat flux (Fig. 3).

The initial heat flux q_0 entering the disk is calculated by the following formula [38]:

$$q_0 = \frac{1-\phi}{2}.\frac{mgv_0z}{2A_d\varepsilon_p} \tag{5}$$

where $z = a/g$ is the braking effectiveness, a is the deceleration of the vehicle (m/s^2), ϕ is the rate distribution of the braking forces between the front and rear axle, A_d disk surface swept by a brake pad (m^2), v_0 is the Initial speed of the vehicle (m/s), ε_p is the factor load distribution on the

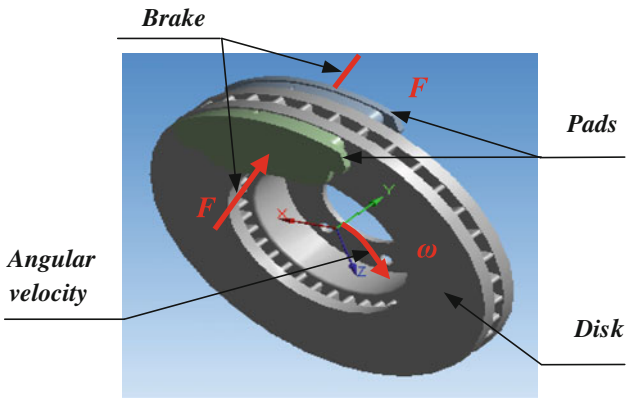

Fig. 1 Disk–pads assembly with forces applied to the disk

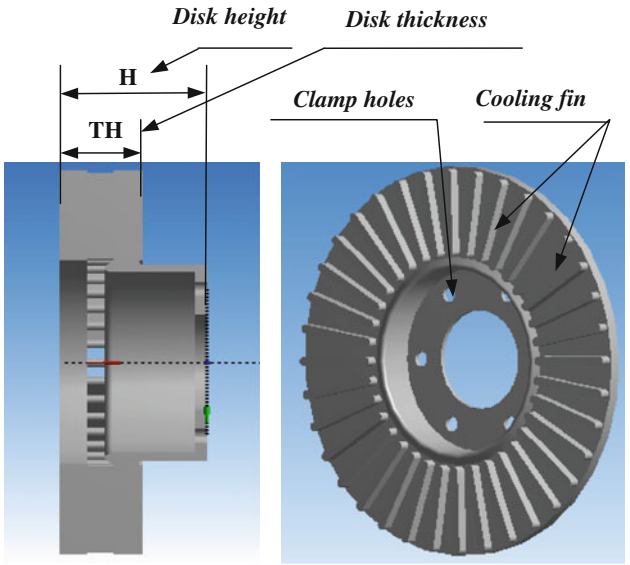

Fig. 2 Geometrical characteristics of the ventilated disk

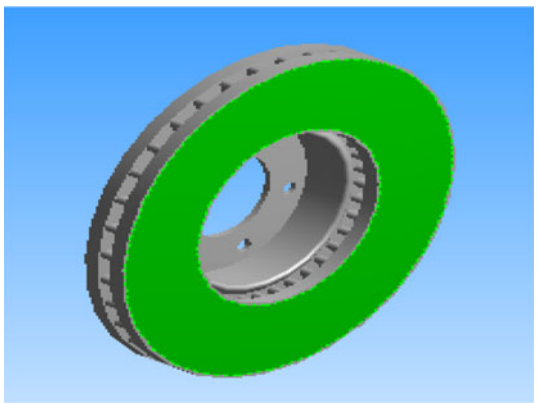

Fig. 3 Application of flux

surface of the disk, m is the mass of the vehicle (kg) and g is the acceleration of gravity (9.81) (m/s^2).

The loading corresponds to the heat flux on the disk surface. The dimensions and the parameters used in the thermal calculation are recapitulated in Table 1. The disk material is gray cast iron with high carbon content [39], with good thermophysical characteristics, and the brake pad has an isotropic elastic behavior, thermomechanical characteristics of which adopted in this simulation of the two parts are recapitulated in Table 2.

The thermal conductivity and specific heat are a function of temperature (Figs. 4, 5).

3 Thermal analysis of the problem

Transient heat conduction in 3D heat-transfer problem is governed by the following differential equation [40]:

$$-\left(\frac{\partial q_x}{\partial x}+\frac{\partial q_y}{\partial y}+\frac{\partial q_z}{\partial z}\right)+Q=\rho C_p\frac{\partial T}{\partial t} \tag{6}$$

where q_x, q_y and q_z are the conduction heat fluxes in x, y, and z directions, respectively; C_p is the specific heat; ρ is the specific mass; Q is the internal heat generation rate per unit volume; and T is the temperature that varies with the coordinates as well as the time t. The conduction heat fluxes can be written in terms of temperature using Fourier's law. Assuming constant and uniform thermal properties, the relations are

Table 1 Parameters of automotive brake application

Inner disk diameter (mm)	66
Outer disk diameter (mm)	262
Disk thickness (TH) (mm)	29
Disk height (H) (mm)	51
Vehicle mass m (kg)	1385
Initial speed v_0 (km/h)	28
Deceleration a (m/s^2)	8
Effective rotor radius R_{rotor} (mm)	100.5
Rate distribution of the braking forces ϕ (%)	20
Factor of charge distribution of the disk ε_p	0.5
Surface disk swept by the pad A_d (mm^2)	35993

Table 2 Thermoelastic properties used in simulation

Material properties	Pad	Disk
Thermal conductivity, k (W/m °C)	5	57
Density, ρ (kg/m^3)	1400	7250
Specific heat, C (J/kg °C)	1000	460
Poisson's ratio, υ	0.25	0.28
Thermal expansion, α (10^{-6}/°C)	10	10.85
Elastic modulus, E (GPa)	1	138
Coefficient of friction, μ	0.2	0.2
Operation conditions		
Angular velocity, ω (rd/s)		157.89
Hydraulic pressure, P (MPa)		1

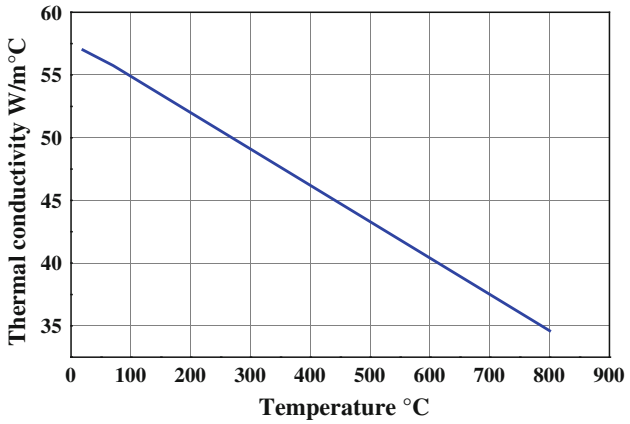

Fig. 4 Thermal conductivity versus temperature

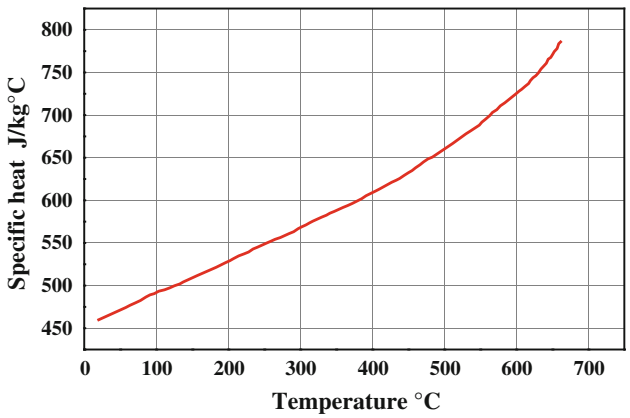

Fig. 5 Specific heat versus temperature

$$q_x = -k_x \frac{\partial T}{\partial x}, \quad q_y = -k_y \frac{\partial T}{\partial y}, \quad q_z = -k_z \frac{\partial T}{\partial z} \tag{7}$$

where k_x, k_y, and k_z are the thermal conductivities in x, y, and z directions, respectively. Heat transfer boundary conditions consist of several heat transfer modes that can be written in different forms. The boundary conditions frequently encountered are as follows [41, 42]:

$$T_s = T_1(x, y, z, t) \tag{8}$$

$$-q_s = h(T_s - T_\infty) \tag{9}$$

where T_1 is the specified surface temperature; q_s the specified surface heat flux (positive into a surface); h is the convective heat transfer coefficient; T_s the unknown surface temperature; and T_∞ the convective exchange temperature.

4 Modeling in ANSYS CFX

The finite volume method consists of three stages: the formal integration of the governing equations of the fluid flow over the entire (finite) control volumes of the solution domain. Then, discretization, involving the substitution of a variety of finite-difference-type approximations for the terms in the integrated equation representing flow processes such as convection, diffusion, and sources. This converts the integral equation into a system of algebraic equations, which can then be solved using iterative methods [43]. The first stage of the process, the control volume integration, is the step that distinguishes the finite volume method from other CFD methods. The statements resulting from this step express the "exact" conservation of the relevant properties for each finite cell volume. This gives a clear relationship between the numerical analog and the principle governing the flow. To enable the modeling of a rotating body (in this case the disk) the code employs the rotating reference frame technique. For the preparation of the mesh of CFD model, one defines initially, various surfaces of the disk in ICEM CFD as shown in the Fig. 6; we used a linear tetrahedral element with 30717 nodes and 179798 elements. In order not to weigh down calculation, an irregular mesh is used in which the mesh is broader where the gradients are weaker (nonuniform mesh; Fig. 7).

The CFD models were constructed and were solved using ANSYS-CFX software package [44]. The model applies periodic boundary conditions on the section sides. As the brake disk is made from sand-casted grey cast iron, the disk model is attached to an adiabatic shaft, the axial length of which spans that of the domain. Air around the disk is considered to be 20 °C, and open boundaries with zero relative pressure were used for the upper lower, and radial ends of the domain. Material data were taken from ANSYS material data library for air at 20 °C. Reference pressure was set to be 1 atm, low turbulence intensity and the turbulent model used was $k - \varepsilon$ (Fig. 8).

The airflow through and around the brake disk was analyzed using the ANSYS CFX software package. The

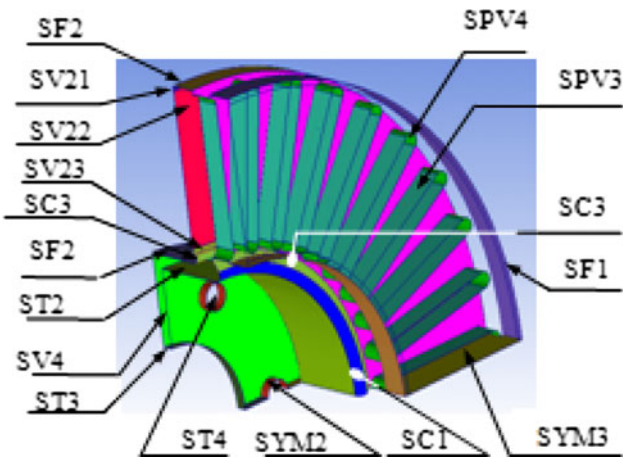

Fig. 6 Definition of surfaces of the ventilated disk

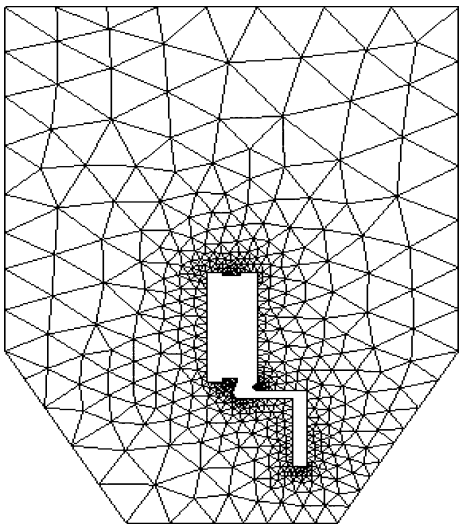

Fig. 7 Irregular mesh in the wall

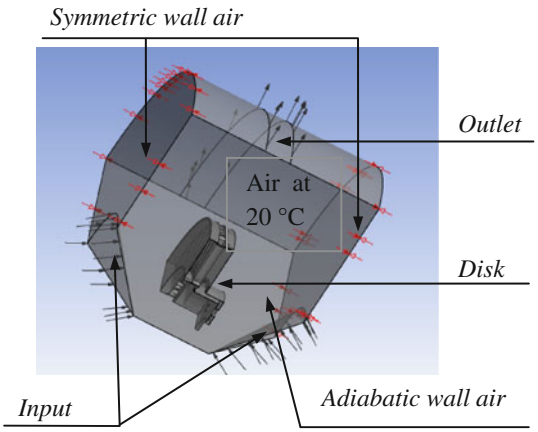

Fig. 8 Brake disk CFD model

ANSYS-CFX solver automatically calculates heat transfer coefficient at the wall boundary. Afterwards the heat transfer coefficients considering convection were calculated and organized in such a way, that they could be used as a boundary condition in thermal analysis. Averaged heat transfer coefficient had to be calculate for all disk using ANSYS CFX Post as it is indicated in Figs. 9 and 10.

(a) Results of the calculation of the heat transfer coefficient h

The heat transfer coefficient is a parameter relates with the velocity of air and the shape of brake disk, and many other factors. In different velocity of air, the heat transfer coefficient in different parts of brake disk changes with time [45]. Heat transfer coefficient will depend on air flow

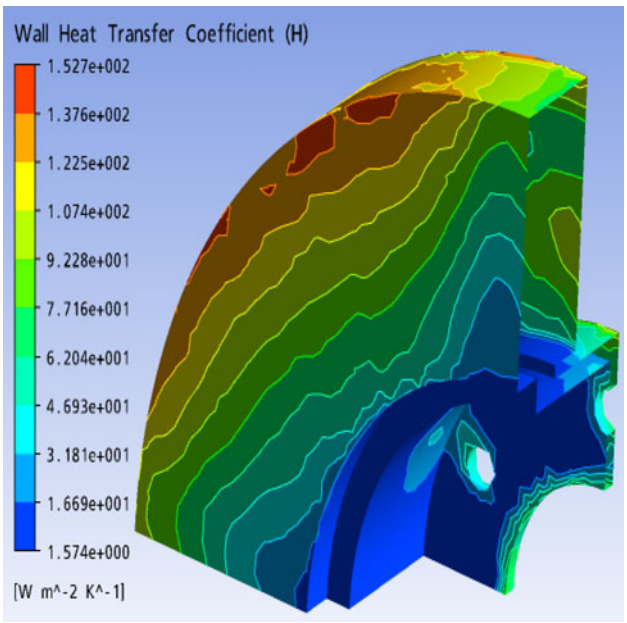

Fig. 9 Distribution of heat transfer coefficient on a full disk in the steady state case (FG 15)

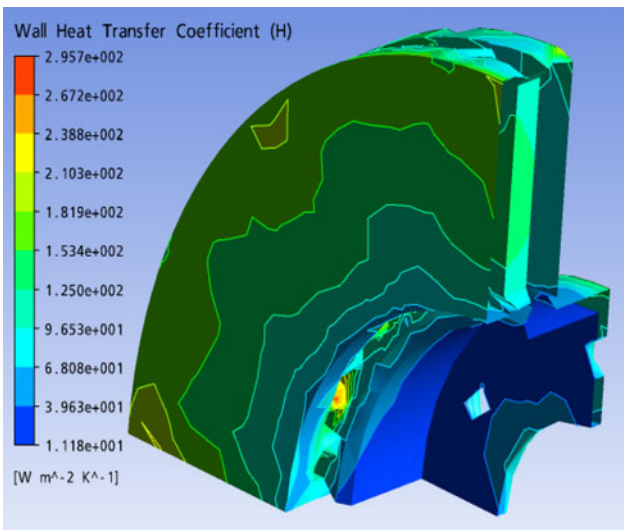

Fig. 10 Distribution of heat transfer coefficient on a ventilated disk in the steady state case (FG 15)

in the region of brake rotor and vehicle speed, but it does not depend on material.

From the comparison between Figs. 11 and 12 concerning the variation of heat transfer coefficient in the nonstationary mode for the two types of design, full and ventilated, one notes that the introduction of the system of ventilation directly influences the value of this coefficient for same surface, which is logically significant because this mode of ventilation results in the reduction in the differences of wall-fluid temperatures.

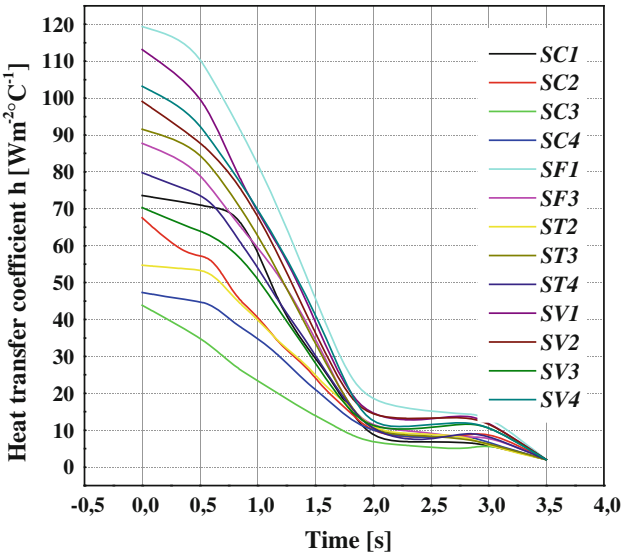

Fig. 11 Variation of heat transfer coefficient (h) of various surfaces for a full disk in transient case (FG 15)

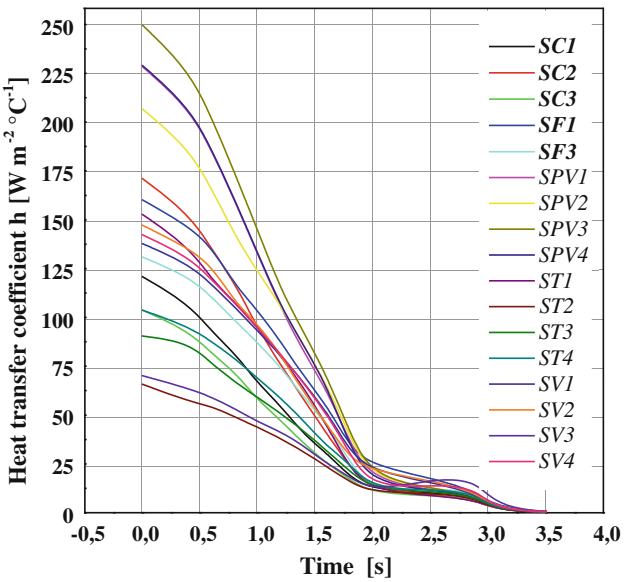

Fig. 12 Variation of heat transfer coefficient (h) of various surfaces for a ventilated disk in transient case (FG 15)

5 Determination of the disk temperature

The modeling of the disk temperature is carried out by simulating a stop braking of a middle class car (braking of type 0).

The characteristics of the vehicle and of the disk brake are listed in Table 1.

The vehicle speed decreases linearly with time until the value 0 as shown in Fig. 13. The variation of the heat flux during the simulation time is represented on the Fig. 14.

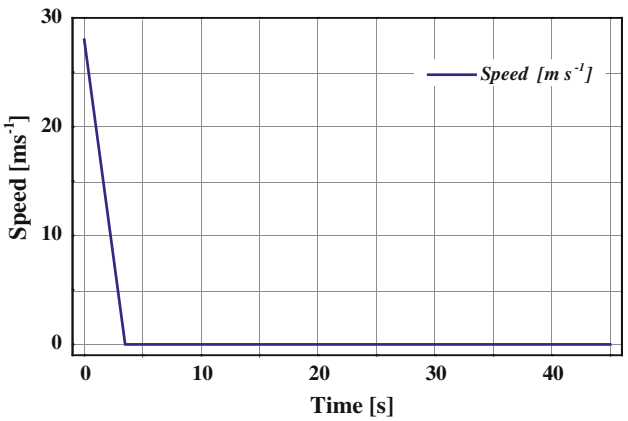

Fig. 13 Speed of braking versus time (braking of type 0)

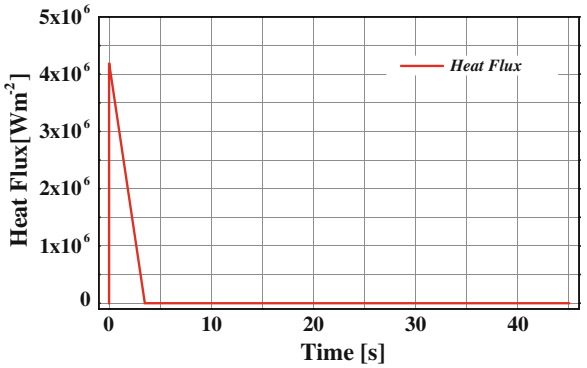

Fig. 14 Heat Flux versus time

6 Meshing of the disk

The elements used for the mesh of the full and ventilated disk are tetrahedral 3D elements with 10 nodes (isoparametric; Fig. 15).

7 Initial and boundary conditions

The boundary conditions are introduced into module ANSYS Workbench [Multiphysics], by choosing the mode of first simulation of the all (permanent or transitory), and by defining the physical properties of materials. These conditions constitute the initial conditions of our simulation. After having fixed these parameters, one introduces a boundary condition associated with each surface.

- Total time of simulation = 45 s
- Increment of initial time = 0.25 s
- Increment of minimal initial time = 0.125 s
- Increment of maximal initial time = 0.5 s
- Initial temperature of the disk = 20 °C
- Materials: Grey Cast iron FG 15.

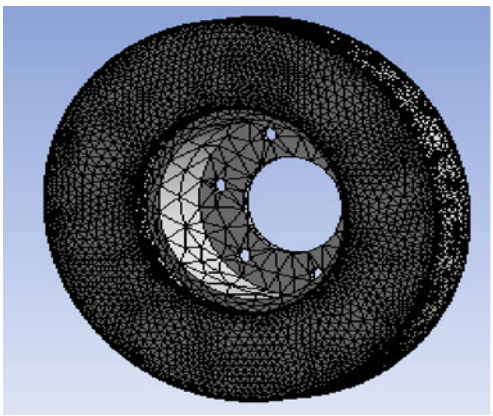

(a)

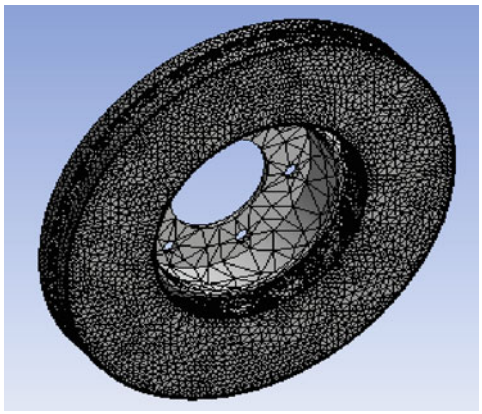

(b)

Fig. 15 Meshing of the disk **a** full disk (172103 nodes—114421 elements) **b** ventilated disk (154679 nodes—94117 elements)

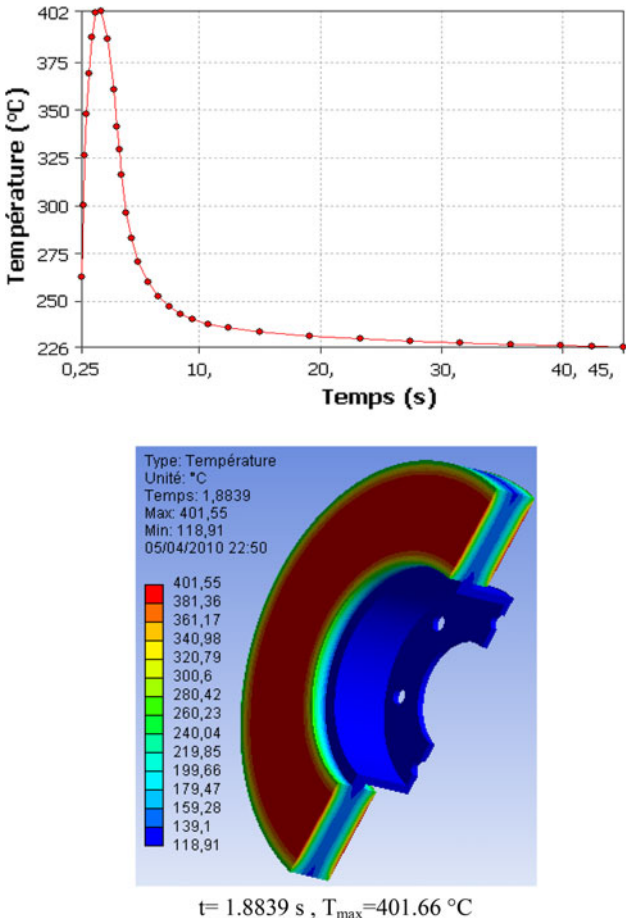

Fig. 16 Temperature distribution of a full disk of cast iron (FG 15)

- *Convection* One introduces the values of the heat transfer coefficient (h) obtained for each surface in the shape of a curve (Figs. 11, 12)
- *Flux* One introduces the values obtained by flux entering by means of the code CFX.

8 Results and discussions

8.1 Influence of construction of the disk

Figures 16 and 17 show the variation in the temperature according to time during the simulation. From the first step, the variation in the temperature shows a great growth which is due to the speed of the physical course of the phenomenon during braking, namely friction, plastic microdistortion of contact surfaces.

For the full disk, the temperature reaches its maximum value of 401.55 °C at the moment $t = 1.8839$ s, and then it falls rapidly up to 4.9293 s, as from this moment and up to the end ($t = 45$ s) of simulation, the variation in the temperature become slow. It is noted that the interval (0–3.5) s represents the phase of forced convection. During this phase, one observes the case of the free convection until the end of the simulation. In the case of the ventilated disk, one observes that the temperature of the disk falls approximately by 60 °C compared with the first case. It is noted that ventilation in the design of the disks of brake plays an important role in producing a better system of cooling.

Figures 18 and 19 respectively show the temperature variation according to the thickness and radius. It is noted that there is an appreciable variation of temperature between the two types of full and ventilated disk. The influence of ventilation on the temperature field appears clearly at the end of the braking ($t = 3.5$ s).

9 Coupled thermo-mechanical analysis

9.1 FE model and boundary conditions

A commercial front disk brake system consists of a rotor that rotates about the axis of a wheel, a caliper–piston

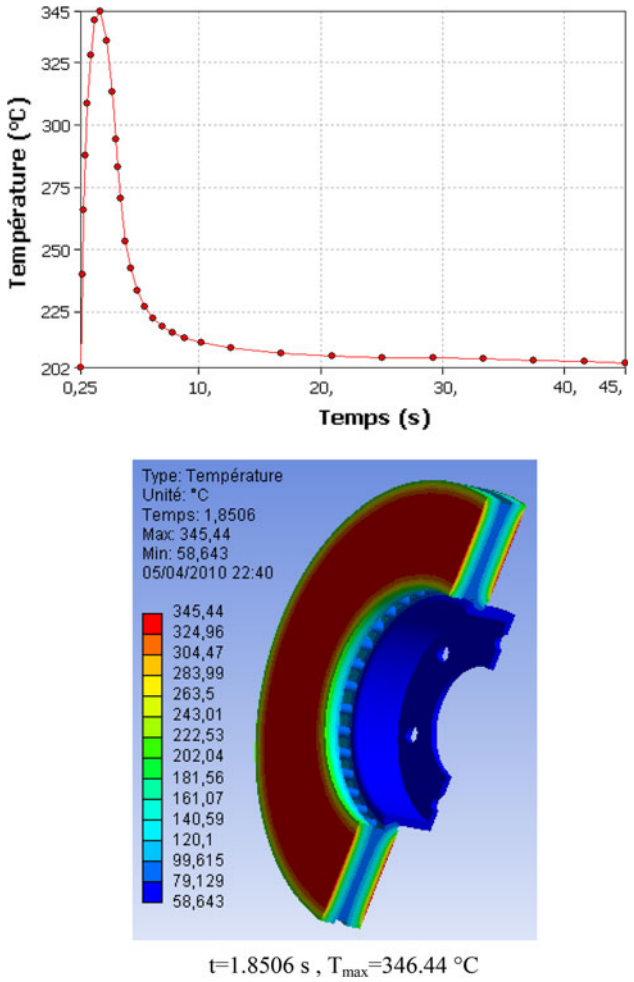

Fig. 17 Temperature distribution of a ventilated disk of cast iron (FG 15)

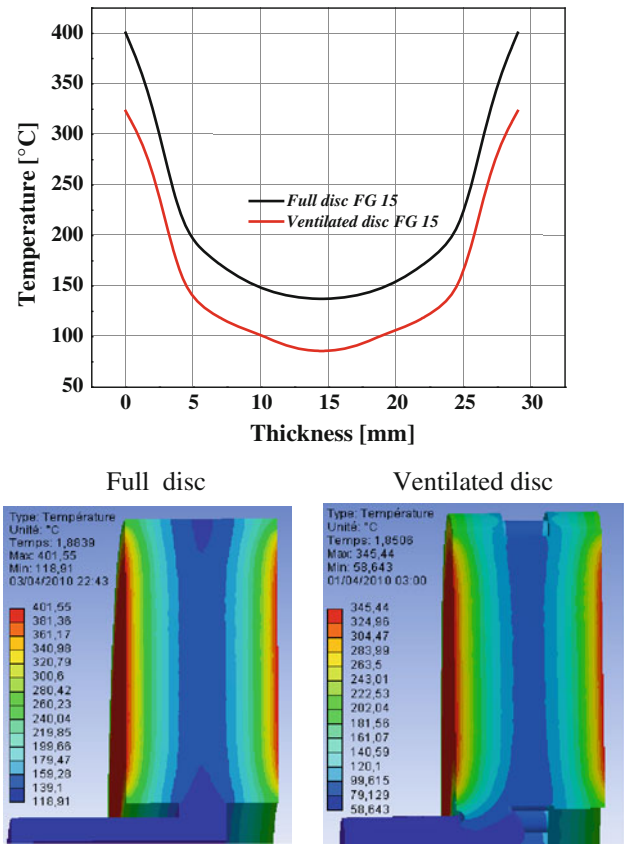

Fig. 18 Temperature variation through the thickness for both designs with same material (FG15)

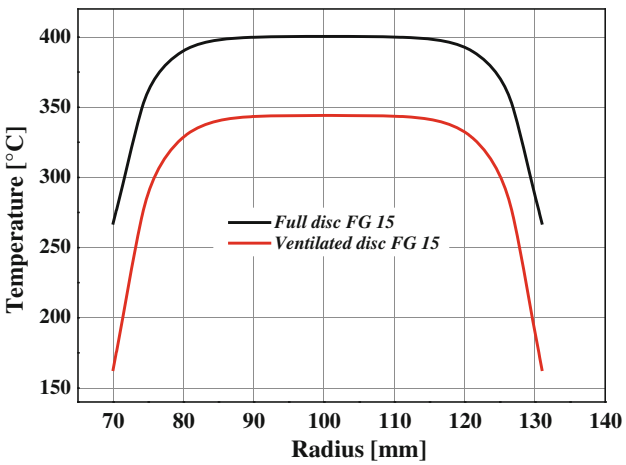

Fig. 19 Temperature variation through a radius or both designs with the same material (FG15)

assembly where the piston slides inside the caliper, which is mounted to the vehicle suspension system, and a pair of brake pads. When hydraulic pressure is applied, the piston is pushed forward to press the inner pad against the disk and simultaneously the outer pad is pressed by the caliper against the disk [46]. Figure 20 shows the FE model and boundary conditions embedded configurations of the model composed of a disk and two pads. The initial air temperature of the disk and pads is 20 °C, and the surface convection condition is applied at all surfaces of the disk and the heat transfer coefficient (h) of 5 W/m^2 °C is applied to the surfaces of the two pads. The FE mesh is generated using 3D tetrahedral element with 10 nodes (solid 187) for the disk and pads. Overall, 185901 nodes and 113367 elements are used (Fig. 21).

In this study, a transient thermal analysis will be carried out to investigate the temperature variation across the disk using ANSYS software. Further structural analysis will also be carried out by coupling thermal analysis.

9.2 Thermal deformation

Due to thermal deformation, contact area and pressure distribution also change. Thermal and mechanical deformations affect each other strongly and simultaneously. The deformation of the disk material gradually increases in the

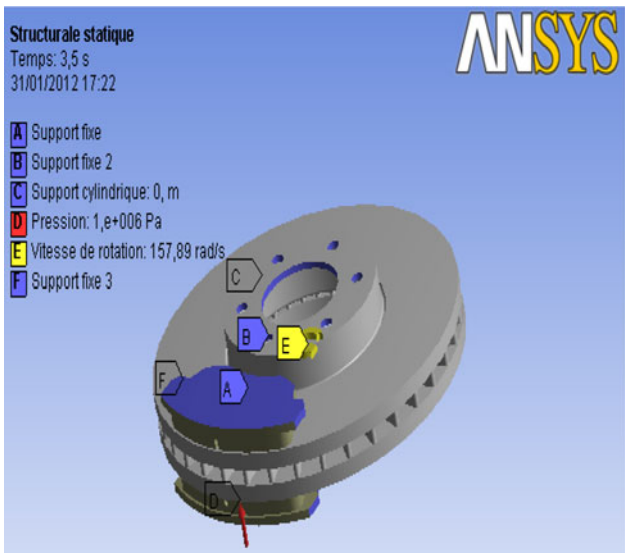

Fig. 20 Boundary conditions and loading imposed on the disk–pads

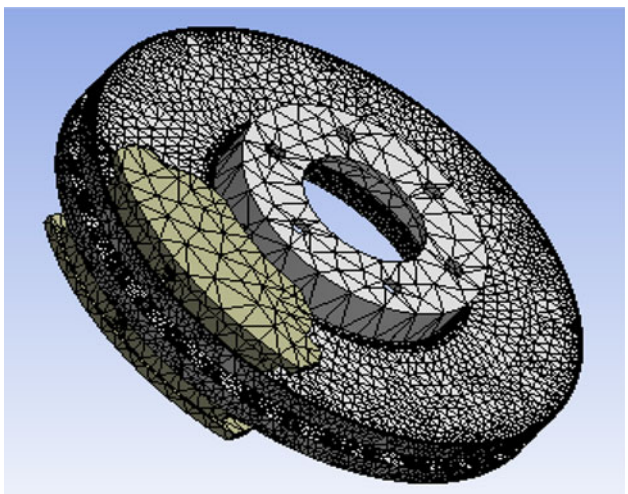

Fig. 21 Refined mesh of the model

radial direction of the disk, and becomes the highest at the circumference region. The deformation of the brake disk due to thermal loading is apparent when viewed through the disk cross section. The thermal deformation of the rotor due to frictional heating produces a non-uniform pressure distribution between the disk and pad. The deformation of the brake disk region is primarily attributed to the thermal expansion of the disk.

Figure 22 gives the distribution of the total distortion in the whole (disk–pads) for various moments of simulation. For this figure, the scale of values of the deformation varies from 0 to 284.55 µm. The value of the maximum displacement recorded during this simulation is at the moment, $t = 3.5$ s, which corresponds to the time of braking. One observes a strong distribution which increases

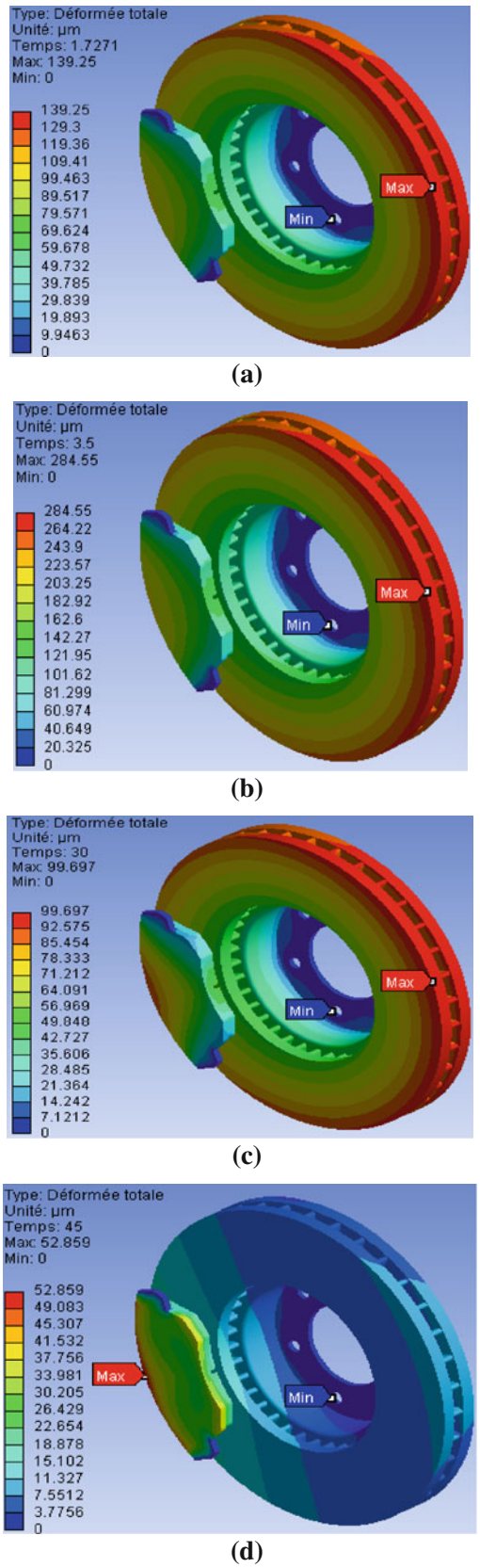

Fig. 22 Total distortion distribution **a** $t = 1.7271$ s, **b** $t = 3.5$ s, **c** $t = 30$ s, **d** $t = 45$ s

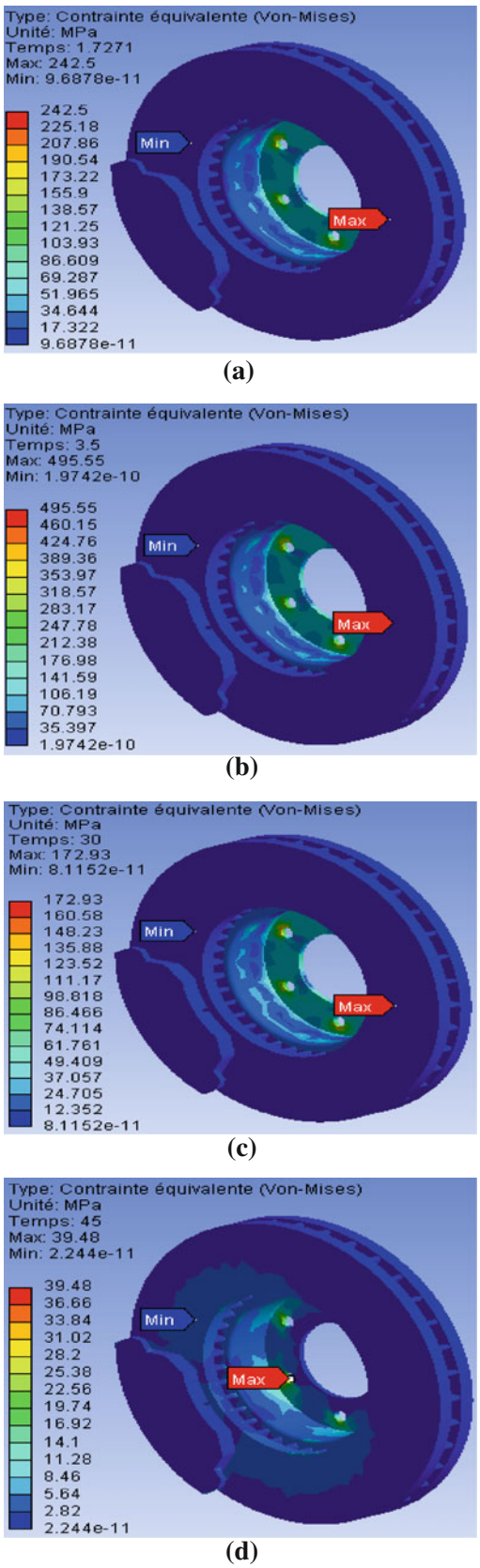

Fig. 23 Von Mises stress distribution **a** $t = 1.7271$ s, **b** $t = 3.5$ s, **c** $t = 30$ s, **d** $t = 45$ s

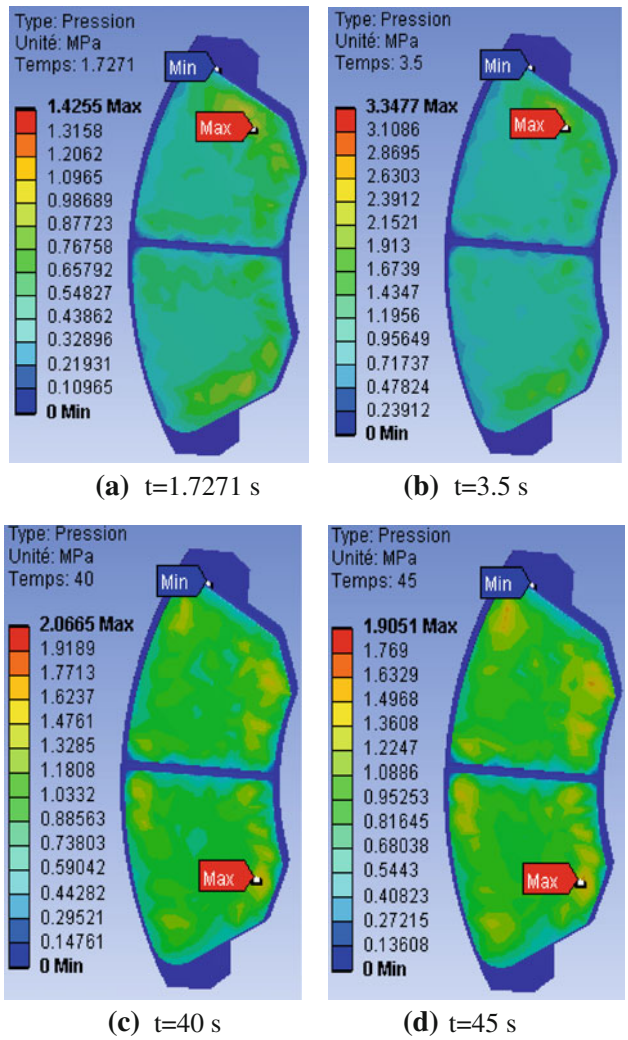

Fig. 24 Contact pressure distribution in the inner pad

with time on the friction tracks, and the external crown and the cooling fins of the disk. Indeed, during a braking moment, the maximum temperature depends almost entirely on the heat storage capacity of disk (on particular tracks of friction); this deformation will generate an asymmetry of the disk following the rise of temperature which will cause a deformation in the shape of an umbrella.

9.3 Von Mises stress distribution

Figure 23 presents the distribution of the constraint equivalent of Von Mises for various moments of simulation, the scale of values varying from 0 to 495.56 MPa. The maximum value recorded during this simulation of the thermomechanical coupling is very significant compared to that obtained with the assistance in the mechanical analysis under the same conditions. One observes a strong constraint on the level of the bowl of the disk. Indeed, the disk

is fixed to the hub of the wheel by screws, thus preventing its movement. In the present of the rotation of the disk and the requests of torsional stress and shears generated at the level of the bowl which are able to create the stress concentrations. The repetition of these effects will lead to risks of rupture on the level of the bowl of the disk.

9.4 Contact pressure

Figure 24 shows the contact pressure distribution in the friction interface of the inner pad taken at various times of simulation. For this distribution, the scale varies from 0 to 3.3477 MPa and reached a value of pressure at the moment $t = 3.5$ s, which corresponds to the null rotational speed. It is also noticed that the maximum contact pressure is located on the edges of the pad decreasing from the leading edge toward the trailing edge from friction. This pressure distribution is almost symmetrical compared with the groove, and it has the same tendency as that of the distribution of the temperature because the highest area of the pressure is located in the same sectors. Indeed, at the time of the thermomechanical coupling of 3D, the pressure produces the symmetric field of the temperature. This last one affects thermal dilation and leads to a variation of the contact pressure distribution.

10 Conclusion

In this article, we have presented the analysis of thermomechanical behavior of the dry contact between the brake disk and pads during the braking process; the modeling is based on the ANSYS 11.0. We have shown that the ventilation system plays an important role in cooling the disks and provides a good high temperature resistance. The analysis results showed that, temperature field and stress field in the process of braking phase were fully coupled. The temperature, Von Mises stress, and the total deformations of the disk and contact pressures of the pads increases as the thermal stresses are apart from the mechanical stress which causes the crack propagation and fracture of the bowl and wear of the disk and pads. Regarding the calculation results, we can say that they are satisfactorily in agreement with those commonly found in the literature investigations. It would be interesting to solve the problem in thermomechanical disk brakes with an experimental study to validate the numerical results, for example, on test benches, in order to demonstrate a good agreement between the model and reality.

Regarding the outlook, there are three recommendations for the expansion of future work related to disk brake that can be done to further understand the effects of thermomechanical contact between the disk and pads, the recommendations are as follows:

- Experimental study to verify the accuracy of the numerical model developed.
- Tribological and vibratory study of the contact disk—pads;
- Study of dry contact sliding under the macroscopic aspect (macroscopic state of the surfaces of the disk and pads).

References

1. Milenković PD et al (2010) The influence of brake pads thermal conductivity on passenger car brake system efficiency. Therm Sci 14(suppl):S221–S230
2. Lee KJ, Barber JR (1994) An experimental investigation of frictionally-excited thermoelastic instability in automotive disk brakes under a drag brake application. J Tribol 116:409–414
3. Altuzarra O, Amezua E, Aviles R, Hernandez A (2002) Judder vibration in disc brakes excited by thermoelastic instability. Eng Comput 19(4):411–430
4. Jang YH, Ahn SH (2007) Frictionally-excited thermoelastic instability in functionally graded material. Wear 262:1102–1112
5. Yi BY, Barber JR, Zagrodzki P (2000) Eigenvalue solution of thermoelastic instability problems using Fourier reduction. Proc R Soc Lond A 456:279–282
6. Nakatsuji T, Okubo K, Fujii T, Sasada M, Noguchi Y (2002) Study on crack initiation at small holes of one—piece brake discs. SAE Technical Paper, Inc, Humble, 2002-01-0926
7. Valvano T, Lee K (2000) An analytical method to predict thermal distortion of a brake rotor. SAE Technical Paper, Inc, Humble, 2000-01-0445
8. Hudson MD, Ruhl RL (1997) Ventilated brake rotor air flow investigation. SAE Technical Paper, Inc, Humble, 01-033
9. Denape J, Laraqi N (2000) Aspect thermique du frottement: mise en évidence expérimentale et éléments de modélisation. Mec Ind 1:563–579
10. Hamraoui M (2009) Thermal behaviour of rollers during the rolling process. Appl Therm Eng 29(11–12):2386–2390
11. Hamraoui M, Zouaoui Z (2009) Modelling of heat transfer between two rollers in dry friction. Int J Therm Sci 48(6):1243–1246
12. Laraqi N (1997) Velocity and relative contact size effect on the thermal constriction resistance in sliding solids. ASME J Heat Transf 119:173–177
13. Yapıcı H, Genç MS, Özısık G (2008) Transient temperature and thermal stress distributions in a hollow disk subjected to a moving uniform heat source. J Therm Stress 31:476–493
14. Laraqi N, Alilat N, Garcia-de-Maria JM, Baïri A (2009) Temperature and division of heat in a pin—on-disc frictional device—exact analytical solution. Wear 266(7–8):765–770
15. Bauzin JG, Laraqi N (2004) Simultaneous estimation of frictional heat flux and two thermal contact parameters for sliding solids. Numer Heat Transf 45(4):313–328
16. Baïri A, Garcia-de-Maria JM, Laraqi N (2004) Effect of thickness and thermal properties of film on the thermal behavior of moving rough interfaces. Eur Phys J Appl Phys 26(1):29–34
17. Mijuca DM, iberna AM, Medjo BI (2005) A new multifield finite element method in steady state heat analysis. Therm Sci 9(1):111–130

18. Gao CH, Lin XZ (2002) Transient temperature field analysis of a brake in a non-axisymmetric three-dimensional model. J Mat Proc Tech 129:513–517
19. Talati F, Jalalifar S (2000) Analysis of heat conduction in a disk brake system. J Heat Mass Transfer 45:1047–1059
20. Naji M, Al-Nimr M, Masoud S (2000) Transient thermal behavior of a cylindrical brake system. J Heat Mass Transf 36:45–49
21. Mosleh M, Blau PJ, Dumitrescu D (2004) Characteristics and morphology of wear particles from laboratory testing of disk brake materials. J Wear 256:1128–1134
22. Mutlu I, Alma MH, Basturk MA (2005) Preparation and characterization of brake linings from modified tannin-phenol formaldehyde resin and asbestos-free fillers. J Mat Sci 40(11):3003–3005
23. Hecht RL, Dinwiddie RB, Wang H (1999) The effect of graphite flake morphology on the thermal diffusivity of gray cast irons used for automotive brake discs. J Mat Sci 34(19):4775–4781
24. Gudmand-Høyer L, Bach A, Nielsen GT, Morgen P (1999) Tribological properties of automotive disc brakes with solid lubricants. J Wear 232(2):168–175
25. Uyyuru RK, Surappa MK, Brusethaug S (2007) Tribological behavior of Al–Si–SiCp composites/automobile brake pad system under dry sliding conditions. J Tribol Int 40(2):365–373
26. Cho MH, Cho KH, Kim SJ, Kim DH, Jang H (2005) The role of transfer layers on friction characteristics in the sliding interface between friction materials against gray iron brake disks. Trib Lett 20(2):101–108
27. Boz M, Kurt A (2007) The effect of Al_2O_3 on the friction performance of automotive brake friction materials. J Tribo Int 40(7):1161–1169
28. Blau PJ, McLaughlin JC (2003) Effects of water films and sliding speed on the frictional behavior of truck disc brake material. Trib Int 36(10):709–715
29. McPhee AD, Johnson DA (2007) Experimental heat transfer and flow analysis of a vented brake rotor. Int J Thermal Sci 47(4):458–467
30. Wallis L, Leonardi E, Milton B, Joseph P (2002) Air flow and heat transfer in ventilated disk brake rotors with diamond and tear-drop pillars. Numer Heat Transf Part A 41:643–655
31. Johnson DA, Sperandei BA, Gilbert R (2003) Analysis of the flow through a vented automotive brake rotor. J Fluids Eng 125:979–986
32. Kang SS, Cho SK (2012) Thermal deformation and stress analysis of disk brakes by finite element method. J Mech Sci Technol 26(7):2133–2137
33. Thilak VMM, Krishnaraj R (2011) Transient thermal and structural analysis of the rotor disc of disc brake. Int J Sci Eng Res 2(8), August-2011, ISSN 2229-5518
34. Zhang L, Yang Q, Weichert D, Nanlin T (2009) Simulation and analysis of thermal fatigue based on imperfection model of brake discs, Beijing Jiaotong University. Proc Appl Math Mech 9:533–534
35. Fiche UIC 541-3 (1993) FREIN—Frein à disques et garnitures de frein à disques, 4^{e} édition, 1 Jury
36. Saumweber E (1969) Temperaturberechnung in Bremsscheiben fürein beliebiges Fahrprogramm,Leichtbau der Verkehrsfahrzeuge, Heft 3, Augsburg
37. Cruceanu C (2007) Frâne pentru vehicule feroviare (Brakes for railway vehicles). MATRIXROM (ed.), Bucureşti, ISBN 978-973-755-200-6
38. Reimpel J (1998) Technologie de freinage. Vogel Verlag, Würzburg
39. Gotowicki PF, Nigrelli V, Mariotti GV (2005) Numerical and experimental analysis of a pegs-wing ventilated disk brake rotor, with pads and cylinders, Jnc: 10th EAEC European Automotive Congress—Paper EAEC05YUAS04—P 5, June
40. Yu H et al (2011) Study on temperature distribution due to freezing and thawing at the Fengman concrete gravity dam. Therm Sci 15(suppl 1):s27–s32
41. Sergerlind LJ (1984) Applied finite element analysis. Wiley, New York
42. Hinton E, Owen DRJ (1981) An introduction to finite element computations. Pineridge Press, Swansea
43. Versteeg HK, Malalasekera W (1995) An introduction to computational fluid mechanics, the finite volume method pearson. Prentice Hall, Harlow
44. ANSYS v.11 User'Manual guide
45. Zhang J, Xia C (2012) Research of the transient temperature field and friction properties on disc brakes. In: Proceedings of the 2012 2nd international conference on computer and information application (ICCIA 2012), pp 201–204
46. Nouby M, Srinivasan K (2009) Parametric studies of disk brake squeal using finite element approach. J Mek 29:52–66